PAPER

Single-component and competitive adsorption of tetracycline and Zn(II) on an NH₄Cl-induced magnetic ultra-fine buckwheat peel powder biochar from water: studies on the kinetics, isotherms, and mechanism†

Tian Ai,[a] Xiaojun Jiang, ⓘD *[a] Qingyu Liu,[b] Linlin Lv[c] and Shujuan Dai*[d]

Single-component and competitive adsorption of tetracycline (TC) and Zn(II) on an NH₄Cl-induced magnetic ultra-fine buckwheat peel powder biochar (NH₄Cl-BHP-char/Fe₃O₄) was investigated in batch experiments. NH₄Cl-BHP-char/Fe₃O₄ exhibited a large surface area of 1119.097 m^2 g^{-1} and a total pore volume of 0.139 cm^3 g^{-1} and was easily separated from aqueous solution using a magnet. Also, adsorption was endothermic, spontaneous, and highly pH-dependent. The optimum pH of the single-component adsorption of TC and Zn(II) was 4.0 and 6.5, respectively, and the optimum pH of co-adsorption was 6.0. The kinetics studies showed the prepared biochar could be rapidly adsorbed within 60 min, and chemical adsorption was dominant. For single-component adsorption, the maximum adsorption capacities of TC and Zn(II) were 106.38 and 151.52 mg g^{-1}, respectively, and they underwent monolayer adsorption on the biochar surface. Moreover, for competitive adsorption, maximum TC and Zn(II) adsorption capacities of 126.58 and 357.14 mg g^{-1} were achieved. Both film diffusion and intra-particle diffusion were found to be significant processes to facilitate adsorption. TC and Zn(II) promoted the adsorption of each other. The proposed biochar could be used repeatedly for at least four cycles. All these results demonstrated that developed NH₄Cl-BHP-char/Fe₃O₄ was regarded as a low-cost alternative adsorbent to remove the heavy metal ions and antibiotic pollutants from water or wastewater.

1   Introduction

China's rapid economic growth and urban expansion generate large amounts of toxic aqueous effluents containing chemical compounds. In particular, heavy metal and antibody pollution in aqueous environments seriously threaten ecological environments and human health, and need to be solved urgently. In the past few decades, the presence of heavy metal ions and antibiotic compounds has been detected at trace concentrations (ng L^{-1} to μg L^{-1}) in surface water and even groundwater in China.[1,2] Persistence and bioaccumulation of these toxic pollutants in aquatic ecosystems can lead to the deterioration of the aquatic ecosystem and seriously endanger human health.[3]

[a]*School of Chemical Engineering, University of Science and Technology Liaoning, Anshan 114051, PR China. E-mail: asjiangxiaojun@163.com; Tel: +86-412-5929641*
[b]*College of Engineering, Shenyang Agricultural University, Shenyang 110161, PR China*
[c]*School of Chemistry and Life Science, Anshan Normal University, Anshan 114005, PR China*
[d]*School of Mining Engineering, University of Science and Technology Liaoning, Anshan 114051, PR China. E-mail: shujuandai@163.com; Tel: +86-412-5928248*
† Electronic supplementary information (ESI) available. See DOI: 10.1039/d0ra02346a

With the increasing public attention to the water environment, it is significant to remove heavy metal ions and antibiotic compounds from wastewater.[4]

Zinc constitutes an essential trace element for the growth of animals and plants. It is essential for the physiological functions of living tissue and regulating biochemical processes.[5] Despite this, excessive zinc ingestion is harmful to health. Eminent health problems, such as stomach cramps, skin irritations, nausea, vomiting, tooth-amalgam, and anemia, are due to a large amount of zinc in the body.[6] Zinc mining, smelting processing, electroplating, and dyes are the primary sources of zinc in wastewater.

Tetracycline (TC) is a sort of broad-spectrum antibiotic utilized for the treatment and prevention of infectious diseases, which is one of the most commonly used antibiotics all over the world.[7] However, the TC is not entirely digested and absorbed by the humans and animals receiving treatment. A significant fraction is excreted through the urine.[8] This compound is hardly metabolized and correctly identified as one of the most resistant drugs in ecosystems.[9] It has been reported that the TC is detected in water sources and even groundwater and drinking water.[10,11] Antibiotics in the water environment mainly come from the discharge of medical wastewater and farming

wastewater. As stated above, the removal of zinc and tetracycline from the water environment is of great importance at the societal level.

Thus, current municipal treatment technologies such as advanced oxidation,[12] adsorptions,[13] membrane separation,[14] ion exchange,[15] and biological treatment[16] have been employed to remove these pollutants from water. Adsorption has been considered as the most effective approach to remove contaminants from aqueous systems with an available adsorbent.[17]

In practice, various adsorbents, especially carbonaceous materials including biochar, have received considerable attention due to their peculiar textural characteristics and potential towards sustainability. They have remarkable adsorption ability for removing antibiotics and heavy metals.[18–20] Biochar (BC), a type of carbon-rich material, produced by pyrolysis of biomass under oxygen-limited conditions.[21]

Some studies suggested that biochar has been recognized as an effective adsorbent owing to its high surface activity.[22] For example, hazelnut shell-based biochar can remove Cr(VI) from aqueous solution.[23] Biochars derived from rice straw, and alligator flag is utilized to reduce the risk posed by sulphamethoxazole.[24] However, the difficulty of recovering or separating the material after its use must be addressed before biochar is widely used to treat water pollution.[25]

In order to improve the separation properties of biochar adsorbent, the development of magnetic biochar has been of great interest recently. Magnetic carrier technology (MCT) enables biochar to separate rapidly from an aqueous environment through a magnetic field. It improves water treatment.[26] Furthermore, high energy ball milling technology has been proved to be considerably useful in the production of magnetic materials.[27] For example, Shan $et\ al.$[22] developed ultrafine magnetic adsorbents for carbamazepine and tetracycline through the ball milling of biochar and activated carbon with magnetite (Fe_3O_4). The results show that the adsorbent is separated magnetically after adsorption.

Buckwheat husks are the dominant byproducts in buckwheat processing, though containing abundant cellulose, lignin, polysaccharide, and flavonoids, are mainly used as pillow fillings currently. Most of them are discarded into the environment or burned in the field, which causes not only the waste of natural resources but also environmental pollution. Consequently, the work was to prepare magnetic ultra-fine buckwheat peel powder biochar by NH_4Cl-induced and ball milling method, which was applied as an adsorbent for TC/Zn(II) removal from ultrapure water.

The competitive adsorption behavior of TC/Zn(II) was studied under different adsorption conditions to refine the adsorption mechanism. The specific objective was to systematically investigate the effects of solution pH, contact time, initial concentration, and temperature on TC/Zn(II) removal by the prepared biochar. Also, the adsorption kinetics, isotherms, and thermodynamics were evaluated. In general, antibiotics and metal ions often coexist in wastewater. Therefore, this innovative work provides a theoretical foundation for a better understanding of their interaction mechanisms.

2 Materials and methods

2.1 Chemicals

TC (98.0% purity, CAS 64-75-5) was purchased from Nanjing Duly Biotech Co., Ltd (Nanjing, China). Table S1† shows its molecular structures and basic physicochemical parameters. Magnetite (Fe_3O_4) powder were purchased from Sinopharm Chemical Reagent Co., Ltd (Shanghai, China). All the other used chemicals were of analytical grade and obtained from Sinopharm Chemical Reagent Co., Ltd (Shanghai, China). All the reagents were used as received without further purification, and all chemical solutions were diluted using ultra-pure water (with the resistivity of 18.2 $M\Omega$ cm^{-1} at 25 °C). Zinc sulphate ($ZnSO_4 \cdot 7H_2O$) was used as a source of divalent zinc. The stock solutions (1000 mg L^{-1}) of TC/Zn(II) were prepared in ultrapure water and stored in brown volumetric flasks at 20 °C in the refrigerator before use. Work solutions of desired concentrations for each test were prepared by diluting the stock solution with ultrapure water.

2.2 Preparation of biochar

Buckwheat peel was obtained from a textile shop in Chengdu, China. Initially, the biomass was rinsed to remove dust and then sun-dried and crushed into 120 mesh (0.125 mm) powder. Finally, keep in a desiccator for further use, abbreviated as BHP.

Biochar was prepared following typical methods reported earlier[28,29] with some modifications. The preparation process of biochar was in a furnace chamber under the nitrogen atmosphere (N_2: 99.99%; flow rate of 350 cm^3 min^{-1}). Briefly, BHP was placed into a box electric furnace and pre-carbonized at a heating rate of 5 °C min^{-1} from room temperature (RT) to 400 °C and then carbonized at this temperature for 1 h. The reactor cooled down to room temperature, and the prepared biochar coded as BHP-char.

BHP-char was repositioned in a box electric furnace, and heated from RT to 300 °C at a heating rate of 5 °C min^{-1} under N_2 atmosphere. Then, pre-carbonize for 1 h at this temperature. After cooling to RT, 5 g biochar was immersed in 150 mL of 2 g L^{-1} ammonium chloride solution. Oscillate for 16 h (oscillating rate: 120 rpm) in a water bath constant temperature oscillator at RT. Next, the modified biochar was filtered and collected to dry in an oven at 60 °C for 2 h. Afterward, the dried sample was heated from RT to 400 °C under N_2 atmosphere (heating rate of 5 °C min^{-1}) for 30 min. The product was withdrawn and allowed to cool. After simply grinding in an agate mortar, seal and dry it for further use, referred hereafter as NH_4Cl-BHP-char.

The NH_4Cl-BHP-char and magnetite (Fe_3O_4) were mixed at a mass ratio of 6.5 : 2 (total 12.8 g), and then the mixture and vibration exciter were added into the millstone. The ball mill equipment operated at a speed of 960 rpm for 10 min at ambient air. Finally, the obtained magnetic biochar was stored in tightly closed bottles before use and named as NH_4Cl-BHP-char/Fe_3O_4. Similar information about magnetic biochar production procedures has been reported in a previously published study.[30]

2.3 Characterization of biochar

Biochar particle size was characterized by a laser particle analyzer (BT-9300S, Bettersize, China). The biochar pH was determined in

a suspension of 0.1 g sample in 10 mL of ultrapure water using a digital pH meter (PHS-3C, Rex Electric Chemical, China). The ash content was measured by heating a certain amount of biochar samples in a muffle furnace at 800 ± 5 °C for 4 h. The elemental (C, H, N) contents in biochar were determined using an elemental analyzer (Vario MICRO cube, Elementar, Germany), and the oxygen (O) content was calculated based on a mass balance (O% = 100%–C%–H%–N%–ash%). The iron (Fe) content was determined by an inductively coupled plasma optical emission spectrometer (ICP-OES) (PQ9000, Jena, Germany).

Thermogravimetric (TG) data were obtained using a thermogravimetric analyzer (Diamond 6300, Perkin Elmer, USA) with a heating rate of 10 °C min^{-1} in the temperature range from 25 to 1000 °C under N$_2$ atmosphere. Surface and pore characteristics of biochar were examined by N$_2$ adsorption at 77 K by a surface area and porosity analyzer (Autosorb iQ$_2$, Quantachrome, USA). The specific surface area, cumulative pore volumes, and average pore diameters were calculated using Brunauer–Emmett–Teller (BET) and Barrett–Joyner–Halenda (BJH) methods based on the N$_2$ adsorption–desorption isotherm data, respectively. The magnetic property of biochar was measured at external magnetic fields ranging between −1.5 T and +1.5 T using a vibrating sample magnetometer (VSM) (Changchun Great Wall Teaching Instrument Co., Ltd model WSM-01, China).

Besides, chemical bonding and groups of adsorbent before and after adsorption were studied by a Fourier transform infrared (FTIR) spectrometer (FT/IR-410, JASCO, Japan) with a resolution of 4.0 cm^{-1} in the wavelength range from 4000 to 400 cm^{-1}. The surface characteristics of obtained biochars were examined by an SEM (Zeiss model ΣIGMA HD/VP, Germany).

2.4 Batch adsorption

Single-component and competitive adsorption behaviors of TC/Zn(II) were illustrated by investigating pH effect, kinetics, isotherms, and thermodynamics. Batch adsorption was tested in the dark in 150 mL stopper conical flasks with 50 mL of TC/Zn(II) solution and 0.025 g biochar on a thermostatic orbital shaker (Orbitek, Scigenics Biotech, India) at 180 rpm. The above conditions remain unchanged throughout the experiment. The pH value of the solution was adjusted using 0.01 mol L^{-1} HCl or 0.01 mol L^{-1} NaOH before adding biochar.

The adsorption was tested in triplicate to make sure the Relative Standard Deviations (RSD) did not exceed 5%. After achieving adsorption equilibrium, the mixtures were magnetically separated under a low magnetic field and then were filtered before analysis in 0.45 μm regenerated cellulose membranes. The remaining concentrations of TC and Zn(II) were monitored by a UV-Vis spectrophotometer (T6, Persee Co., Ltd, China) and a flame atomic absorption spectrometer (FAAS) (AAnalysis200, PerkinElmer, USA), respectively.

TC detection wavelength was set at 276 nm. Text S1† shows the standard curves of TC and Zn(II). Control experiments with no adsorbent indicated that the adsorption of TC and Zn(II) onto flasks and regenerated cellulose membranes was negligible. Accordingly, the equilibrium adsorption capacity q_e (mg g^{-1}) was calculated based on

$$q_e = \frac{(C_0 - C_e)V}{W} \quad (1)$$

where C_0 (mg L^{-1}) and C_e (mg L^{-1}) are the initial and equilibrium of TC and Zn(II), respectively; V (L) is the volume of the solution; W (mg) the dry mass of the biochar adsorbent.

2.5 The influence of solution pH

The pH influence on the adsorption of TC/Zn(II) onto biochar adsorbents was investigated at pH 4.0 to 9.0. Other operating conditions were as follows: initial TC/Zn(II) concentrations of 25 mg L^{-1}, adsorbent concentrations of 0.5 g L^{-1}, temperature of 25 °C, and contact time of 120 min.

In the work, at pH < 4.0 or pH > 9.0, there was leaching of iron, which implied that this magnetic material was only stable at pH 4.0 to 9.0. Therefore, the adsorption was highest at pH 4.0 to 9.0, considered as the optimum for the adsorption studies and subsequent experiments.

2.6 Adsorption kinetics

Equilibrium adsorption was studied for a pre-determined time interval (between 0 min to 240 min) to investigate the influence of contact time. Other operating conditions were as follows: the single-component adsorption of TC at pH 4.0, the single-component adsorption of Zn(II) at pH 6.5, the co-adsorption of TC/Zn(II) at pH 6.0, the initial TC/Zn(II) concentrations of 25 mg L^{-1}, the adsorbent concentrations of 0.5 g L^{-1}, and the temperature of 25 °C.

The kinetic models can provide valuable information for reaction pathways: adsorption rate, and adsorbent/adsorbate interaction (physisorption or chemisorption). Thus, the pseudo-first-order model and pseudo-second-order model were used to analyze the kinetic adsorption data. Also, possible adsorption mechanisms were evaluated by intra-particle diffusion and film diffusion equation. Text S2† shows the theory behind each method.

2.7 Adsorption isotherms

Adsorption isotherm was studied with initial TC/Zn(II) concentrations varying from 0.5 to 100 mg L^{-1}. Other operating conditions were as follows: the single-component adsorption of TC at pH 4.0, the single-component adsorption of Zn(II) at pH 6.5, co-adsorption of TC/Zn(II) at pH 6.0, the adsorbent concentrations of 0.5 g L^{-1}, the temperature of 25 °C, and the contact time of 120 min.

Adsorption isotherm models were extended to describe information about the distribution of adsorbate between the liquid and solid phases at equilibrium concentrations. Thus, the four most common adsorption models, i.e., Langmuir, Freundlich, Temkin, and Dubinin–Radushkevich (D–R) isotherm models, were employed to assess the adsorption process. Text S3† shows the detailed hypotheses and equations of the four models.

2.8 Adsorption thermodynamics

Adsorption thermodynamics was tested at 20, 25, 30, 35, and 40 °C. Other operating conditions were as follows: the single-component adsorption of TC at pH 4.0, the single-component

adsorption of Zn(ii) at pH 6.5, the co-adsorption of TC/Zn(ii) at pH 6.0, the adsorbent concentrations of 0.5 g L^{-1}, the initial TC/Zn(ii) concentrations of 25 mg L^{-1}, and the contact time of 120 min. A study on the effect of temperature on adsorption will extend the knowledge of thermodynamic parameters, including the standard Gibb's free energy ($\Delta G°$), the enthalpy change ($\Delta H°$), and the entropy change ($\Delta S°$).[31] Text S4† shows the equations for calculating the three parameters.

2.9 Regeneration and recycling of NH$_4$Cl-BHP-char/Fe$_3$O$_4$

Adsorption–desorption was tested under the following conditions to evaluate the recyclability of the NH$_4$Cl-BHP-char/Fe$_3$O$_4$: co-adsorption of TC/Zn(ii) at pH 6.0, the adsorbent concentrations of 0.5 g L^{-1}, the initial TC/Zn(ii) concentrations of 25 mg L^{-1}, the temperature of 25 °C, and the contact time of 120 min.

After adsorption, NH$_4$Cl-BHP-char/Fe$_3$O$_4$ was magnetically collected from the solution. Then ultrasonically wash for 10 min with 20 mL of methanol (regenerant). Finally, the obtained biochar was dried at 60 °C and used for the next adsorption–desorption experiment. Adsorption–desorption procedures were repeated four times by the same NH$_4$Cl-BHP-char/Fe$_3$O$_4$.

3 Results and discussion

3.1 Characterization of biochar adsorbents

Fig. S1 and Table S2† show the particle-size distribution of BHP-char and NH$_4$Cl-BHP-char/Fe$_3$O$_4$, respectively. The mean particle size of NH$_4$Cl-BHP-char/Fe$_3$O$_4$ was observed to be 3.889 μm, much lower than that of BHP-char (101.1 μm). The ball milling process was applied to reduce the particle size of biochar.

Table 1 shows the elemental composition and atomic ratio parameters of BHP-char and NH$_4$Cl-BHP-char/Fe$_3$O$_4$. Both biochar samples were carbon-rich and belonged to typical of pyrolyzed biomass.

Also, the %Fe measured using acid digestion in BHP-char was negligible while NH$_4$Cl-BHP-char/Fe$_3$O$_4$ had 19.16% of Fe. Fe$_3$O$_4$ could be the primary source of Fe. For NH$_4$Cl-BHP-char/Fe$_3$O$_4$, the two ratios were 0.0254 and 0.203 for H/C and O/C, respectively, much lower than the rates for BHP-char of 0.0271 and 0.285. It indicated that intense dehydrogenation and deoxygenation reactions occurred during the modification of biochar, and aromaticity and hydrophobicity decreased to some extent.[21]

Fig. 1 shows the magnetization curves of NH$_4$Cl-BHP-char/Fe$_3$O$_4$. NH$_4$Cl-BHP-char/Fe$_3$O$_4$ exhibits a saturation magnetization
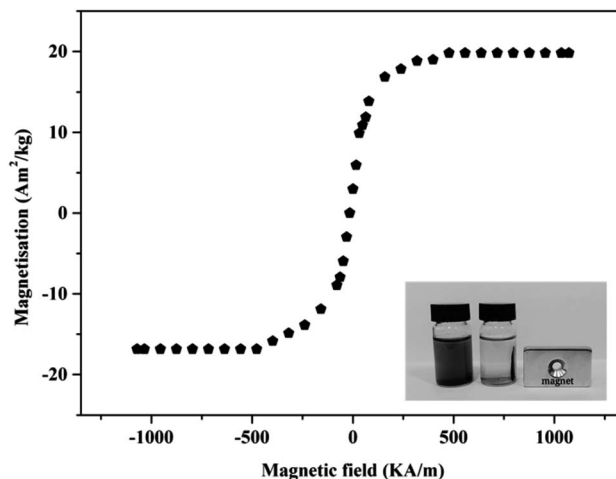
Fig. 1 Magnetic hysteresis cycles of NH$_4$Cl-BHP-char/Fe$_3$O$_4$ (inset plots showing the magnetic separation NH$_4$Cl-BHP-char/Fe$_3$O$_4$ after TC and Zn^{2+} adsorption).

of 19.8 A m^2 kg^{-1}, with good magnetism. Consequently, it could be easily separated from an aqueous solution using a permanent magnet after adsorption (Fig. 1, inset).

Table 2 shows the structural properties of biochar materials used in the work. NH$_4$Cl chemically-activated magnetic biochar exhibits the relatively large surface area (1119.097 m^2 g^{-1}) and the total pore volume (0.139 cm^3 g^{-1}), which are better than those of unmodified biochar (869.359 m^2 g^{-1} and 0.123 cm^3 g^{-1}, respectively). Fe$_3$O$_4$ particles produced in the milling process might have blocked some pores in the biochar, which leads to the decreased surface area.[22] However, the NH$_4$Cl combustion in the process of preparing the modified biochar produces excess gas, which destroys carbon texture to generate a large number of holes.[29] Therefore, the high surface area and pore volume of NH$_4$Cl-BHP-char/Fe$_3$O$_4$ play an essential role in adsorbing relatively large TC molecules.

The thermal stability of BHP-char and NH$_4$Cl-BHP-char/Fe$_3$O$_4$ was monitored by the thermogravimetric analysis (TGA) under inert atmosphere (nitrogen). Fig. S2† shows the thermogravimetric derivative (DTG) curves. The TG curves indicate that the thermal stability of modified biochar decreases slightly after ball milling. DTG curves show that two biochars are lost free water around 41 °C. The broad peaks at 188, 462, and 610 °C may be due to the decomposition of carboxyl and carbonyl groups, which involve the pyrolysis of cellulose, hemicellulose, and lignin in buckwheat peel powder biochar. Furthermore, NH$_4$Cl-BHP-char/Fe$_3$O$_4$ contains a large amount

Table 1 The information of elemental composition of the biochar adsorbents

| Adsorbent | pH | Ash (%) | Elemental composition (%, mass based) | | | | | H/C | O/C |
			C	H	O	N	Fe		
BHP-char	7.52	15.66	60.58	1.64	17.24	4.88	0.02	0.0271	0.285
NH$_4$Cl-BHP-char/Fe$_3$O$_4$	7.77	33.13	51.19	1.30	10.41	3.97	17.11	0.0254	0.203

Table 2 The surface properties of the biochar adsorbents

Adsorbent	BET surface area ($m^2\ g^{-1}$)	BJH cumulative pore volume ($cm^3\ g^{-1}$)	BJH average pore diameter (nm)
BHP-char	869.359	0.123	3.054
NH_4Cl-BHP-char/Fe_3O_4	1119.097	0.139	3.417

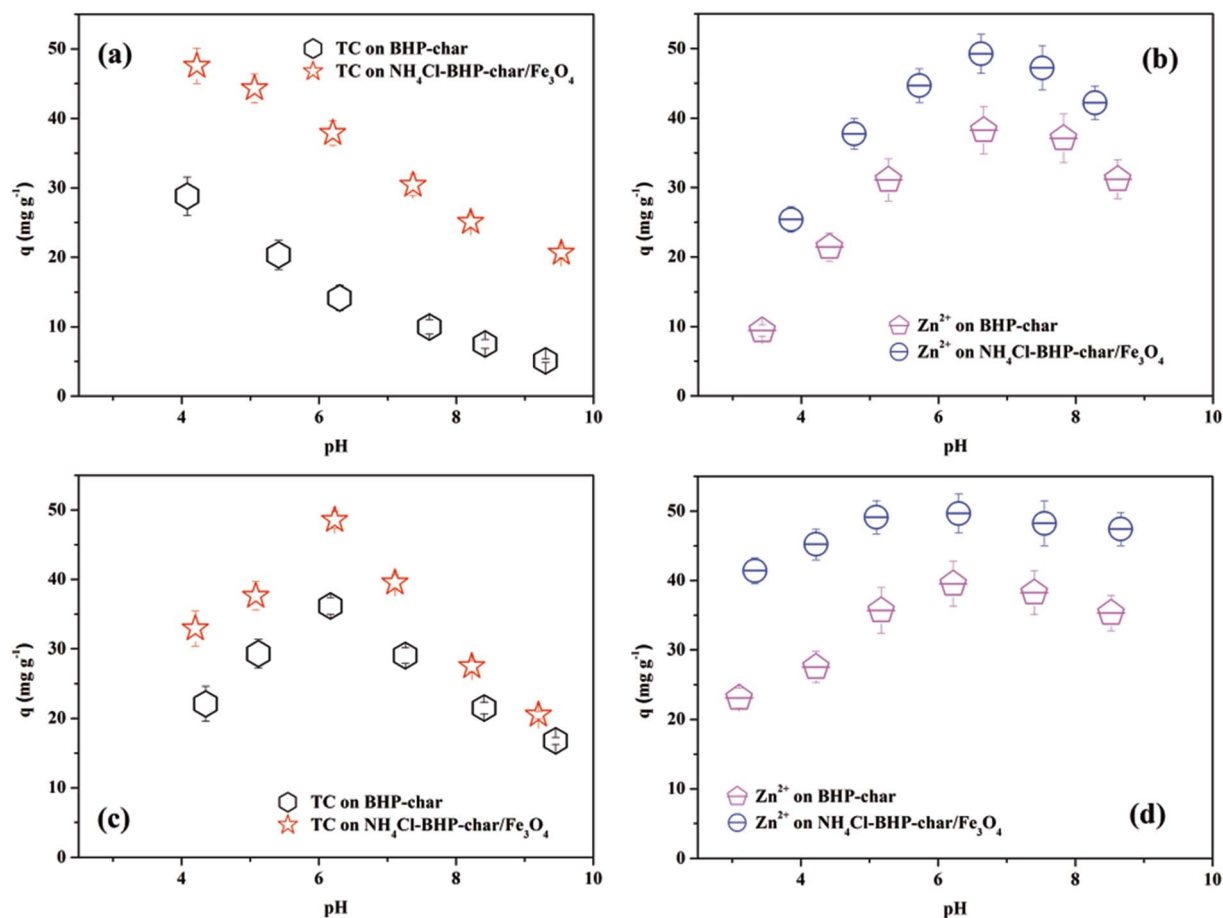**Fig. 2** Effect of equilibrium pH on adsorption of TC and Zn^{2+} by BHP-char and NH_4Cl-BHP-char/Fe_3O_4 ((a and b) single-component adsorption system, (c and d) co-adsorption system). Conditions: initial TC/Zn(II) concentrations 25 mg L^{-1}, adsorbent concentrations 0.5 g L^{-1}, temperature 25 °C, contact time 120 min.

of magnetite. The sharp and narrow peak at 813 °C is due to the reduction reaction of Fe_3O_4 with C to form CO_2.

Fig. S3† shows the surface morphology and the microstructures of BHP-char, NH_4Cl-BHP-char, and NH_4Cl-BHP-char/Fe_3O_4. Fig. S3(a) and (d)† show the BHP-char displays a compact net structure surface. After activating with NH_4Cl, NH_4Cl-BHP-char exhibits a highly wrinkled and honeycomb-like structure, indicating the development of pore structure leads to the enhancement in exposed surface area (See Fig. S3(b) and (e)†). A large number of pores form on the honeycomb-like structure, which is related to the gasification reaction during NH_4Cl activation.

Fig. S3(c) and (f)† show that the particle size of NH_4Cl-BHP-char/Fe_3O_4 decreases obviously after ultra-fine milling, and the

honeycomb-like structure is not undermined by Fe_3O_4 loading. Furthermore, Fe_3O_4 is not uniformly distributed on the surface of NH_4Cl-BHP-char/Fe_3O_4, which is beneficial to magnetic separation.

3.2 Effect of solution pH

Solution pH is an essential parameter for controlling surface adsorption processes because it might affect the chemical speciation of TC/Zn(II) to change their adsorption properties on biochar adsorbent.[32] Based on the previous research, magnetic biochar is only stable at pH 4–9.[30] Besides, the point of zero charges of both biochars determined by reverse mass titration method[33] is much less than 4, indicating that their surface is

negatively charged at pH 4–9. In the absence of iron leaching, the pH value with maximum adsorption capacity is considered as the optimum to be used in subsequent experiments. Fig. 2 shows the effects of solution pH on the adsorption of TC/Zn(II) on BHP-char and NH₄Cl-BHP-char/Fe₃O₄.

TC molecules contain three dissociated groups, *i.e.*, tricarbonyl group ($pK_{a1} = 3.30$), phenolic diketone moiety ($pK_{a2} = 7.68$) and dimethylamino group ($pK_{a3} = 9.68$).[34] Depending on the solution pH, its conformations can form three species, including cationic species (TCH⁺, pH < 3.32), zwitterionic species (TCH±, 3.32 < pH < 7.78) or anionic species (TCH⁻, pH > 7.78). Therefore, at pH 4–9, TC form is dominated by TCH± and TCH⁻. Zinc ions co-exist in different forms, such as Zn^{2+} and $Zn(OH)^+$, and the stability of these forms is dependent on the pH in aqueous solution. Below pH 6.5, Zn^{2+} is the dominant species. The increasing pH shifts the concentration of Zn^{2+} to $Zn(OH)^+$ and other forms like $Zn(OH)_2$.

In Fig. 2, the same trends are observed for TC/Zn(II) adsorption on BHP-char and NH₄Cl-BHP-char/Fe₃O₄, and NH₄Cl-BHP-char/Fe₃O₄ exhibits higher adsorption capacities than BHP-char under the same experimental conditions. Some mechanisms may occur in the adsorption process involving TC, including electrostatic interaction, hydrogen bonding formation, electron donor–acceptor, and π–π dispersion interaction.[35]

In a single-component adsorption system of TC (see Fig. 2(a)), the adsorption capacity of BHP-char and NH₄Cl-BHP-char/Fe₃O₄ decreases sharply from 28.80 and 47.55 mg g⁻¹ to 5.10 and 20.61 mg g⁻¹ as the pH increased from 4 to 9, respectively. Adsorption becomes unfavorable due to the electrostatic repulsion between TC anion species and the negative charge of the biochar surface as pH increased. It is hypothesized that hydrogen bonding and hydrophobic interactions play a role in the adsorption of TC. Therefore, pH 4 is considered as the optimum for the single-component adsorption of TC.

In a single-component adsorption system of Zn(II) (see Fig. 2(b)), for both biochars, the adsorption capacity of Zn(II) increases as the pH of the solution increases; however, it declines after reaching maximum adsorption at pH 6.5. The maximum adsorption of BHP-char and NH₄Cl-BHP-char/Fe₃O₄ is 38.26 and 49.23 mg g⁻¹, respectively.

The lower adsorption at acid pH values may be attributed to a large number of hydrogen ions (H_3O^+) occupied by the biochar
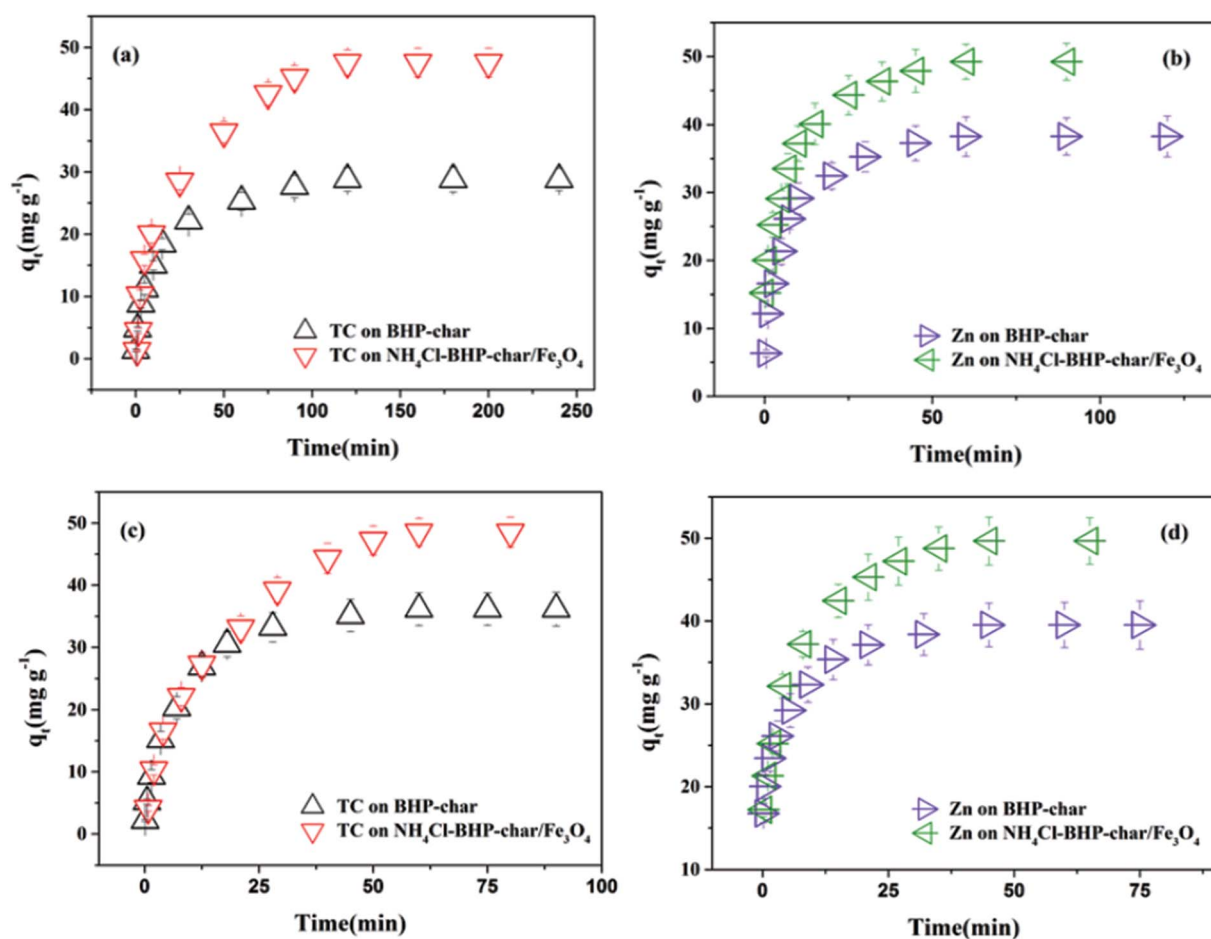

Fig. 3 Effect of contact time on adsorption of Zn^{2+} and TC by BHP-char and NH₄Cl-BHP-char/Fe₃O₄ ((a and b) single-component adsorption system, (c and d) co-adsorption system). Conditions: pH of single-component adsorption of TC was 4.0, pH of single-component adsorption of Zn(II) was 6.5, pH of co-adsorption of TC/Zn(II) was 6.0, initial TC/Zn(II) concentrations 25 mg L⁻¹, adsorbent concentrations 0.5 g L⁻¹, temperature 25 °C.

Table 3 Comparison of TC and Zn(II) maximum capacity onto different biochars

Adsorbent	Abbreviation	Surface area (m² g⁻¹)	Adsorption conditions	C_0 (mg L⁻¹)	q_m (mg g⁻¹) TC	Zn(II)	References
Poplar biochars	KBC300	1.61	pH 5.0, temperature 298 K, contact time 72 h	10–50	21.17	—	40
Rice straw	R600	21.69	Temperature 25 °C, contact time 24 h	0.5–32	14.185	—	41
Swine manure	M600	10.56	Temperature 25 °C, contact time 36 h		8.125	—	42
Pine cone	PC-SO₃H	4.55	pH 3.5, temperature 298 K, contact time 24 h	50–500	357	—	43
Palm kernel cake	CPMn	56.2	Temperature 303.15 K, contact time 260 min	65–90	—	22.38	44
Beech wood chips	BC A	27.24	pH 5.65, temperature 22 °C, contact time 24 h	10–75	—	0.97	45
Garden green waste residues	BC B	31.54			—	2.23	
Banana peels	CMB	323.2	pH 6.0, temperature 298 K, contact time 120 min	50–200	—	72.8	
Buckwheat peel powder	BHP-char	869.359	pH 6.0, temperature 25 °C, contact time 2 h	0.5–100	76.92	192.31	This study
	NH₄Cl-BHP-char/Fe₃O₄	1119.097			126.58	357.14	This study

surface, thereby reducing the binding of Zn(II) on the adsorbent surface. As pH increased, electrostatic repulsion and the competing effect of H_3O^+ decreases due to the reduction of positive charge density on the biochar surface, resulting in an enhancement of the adsorption of Zn(II). However, with further increase in pH, the continuous formation of insoluble zinc compounds decreases the concentration of free zinc ion, thereby decreasing the adsorption capacity. Based on these results, pH 6.5 is selected for the subsequent experiments.

In a co-adsorption system of TC and Zn(II) (See Fig. 2(c) and (d)), Zn(II) dramatically affects the adsorption of TC by biochar, and the adsorption trend of TC and Zn(II) is similar. Under acidic conditions, the adsorption capacity of TC in the co-adsorption system is lower than that in the single-component adsorption system. It increases with the increasing pH and declines after reaching maximum adsorption at pH 6.0. Compared with the single-component adsorption of Zn^{2+}, TC in solution has little effect on the adsorption of Zn^{2+} due to the formation of TC–Zn^{2+} complexes in the aqueous solution or the role of surface bridging (TCH⁻ or Zn^{2+}).

Furthermore, H_3O^+ compete for adsorption sites under acidic conditions, which makes the adsorption effect insignificant. Nevertheless, as pH increases to 6.0, the promotion effect of adsorption obviously becomes more robust, and the adsorption capacities of TC (BHP-char 36.16 mg g⁻¹ and NH₄Cl-BHP-char/Fe₃O₄ 48.55 mg g⁻¹) and Zn^{2+} (BHP-char 39.51 mg g⁻¹ and NH₄Cl-BHP-char/Fe₃O₄ 49.66 mg g⁻¹) reach the maximum. When the solution pH increases further, the adsorption capacity and affinity of TC and Zn^{2+} are weakened drastically due to the influence of deprotonation and electrostatic repulsion.[36] Thus, in the co-adsorption experiment, pH 6.0 is optimum.

3.3 Adsorption kinetics

Fig. 3 shows the evolution of TC/Zn(II) adsorption *versus* time onto BHP-char and NH₄Cl-BHP-char/Fe₃O₄. All curves have a similar form. In a single-component adsorption system (see Fig. 3(a) and (b)), equilibrium is reached after 60 min for Zn(II) and after 120 min for TC. In the co-adsorption system (see Fig. 3(c) and (d)), the adsorption becomes faster, and in particular for TC that the adsorption reaches equilibrium within about 60 min. This excellent performance can be ascribed to the bridged complexes formed by TC/Zn(II) in aqueous solution.[37]

The widely used pseudo-first-order and pseudo-second-order models were employed to correlate the kinetics data, which could compare the adsorption kinetics of TC/Zn(II) onto BHP-char or NH₄Cl-BHP-char/Fe₃O₄. Table S3† shows the corresponding kinetic parameters.

In single-component adsorption system, pseudo-second-order model well fitted the kinetic data with higher R^2 values (0.9929, 0.9959, 0.9977 and 0.9931) than pseudo-first-order model (R^2 = 0.9759, 0.9921, 0.9798 and 0.9791). Moreover, the calculated adsorption capacity ($q_{e,cal}$) was in good agreement with the experimental adsorption capacity ($q_{e,exp}$). As a result, chemisorption referred to the major adsorption mechanism, electron donor–acceptor and π–π dispersion interaction acted simultaneously in the adsorption of adsorbate on biochar.[38,39]

In the co-adsorption system, the pseudo-second-order model ($R^2 = 0.9919$, 0.9990, 0.9970 and 0.9959) was better for predicting experimental data than the pseudo-first-order model ($R^2 = 0.9852$, 0.9798, 0.9806 and 0.9934). Besides, $q_{e,cal}$ estimated by the pseudo-second-order kinetic model was extremely close to $q_{e,exp}$. Both physisorption and chemisorption simultaneously controlled the adsorption process, and the latter was relatively dominant.

3.4 Adsorption isotherm

Four widely used Langmuir, Freundlich, Temkin, and D–R models were adopted for fitting the adsorption equilibrium data to gain further insights into the adsorption mechanism of TC/Zn(II) onto NH$_4$Cl-BHP-char/Fe$_3$O$_4$. Table S4† shows the calculated isotherm parameters.

In the single-component adsorption system, based on the R^2 values, the isotherm equations correlated the data in the following increasing order: Langmuir > Freundlich > Temkin > D–R. Compared with the Freundlich model, the Langmuir isotherm model had higher R^2 values (0.9913, 0.9951, 0.9966, and 0.9977). Hence, the higher likelihood of occurrence of monolayer coverage of Zn^{2+} and TC molecules on the biochar surface was expected.

For TC and Zn^{2+}, values of q_L calculated by the Langmuir isotherm equation on NH$_4$Cl-BHP-char/Fe$_3$O$_4$ were 106.38 and 151.52 mg g^{-1}, which were ~2.68 and ~1.38 times that of BHP-char (39.68 and 109.89 mg g^{-1}), respectively. The adsorption performance of biochar prepared by ammonium chloride activation and magnetic ultra-fine ball milling had a significant improvement.

Different from the single-component adsorption system, the Freundlich model in the co-adsorption system was more suitable for TC/Zn(II) adsorption than the Langmuir. Also, based on the values of q_L, the adsorption performance of the co-adsorption system was better than that of the single-component adsorption system. The above results showed that the adsorption of TC and Zn^{2+} on biochar adsorbent was multilayer adsorption on a heterogeneous surface, and the co-occurrence of two adsorbates promoted the adsorption of each other. Table 3 shows the comparison between several biochars applied for TC and Zn(II) removal concerning surface area, adsorption conditions, and maximum adsorption capacity.

The Temkin model shows β_T values are less than 1 in both adsorption systems, which indicates that the adsorption reaction of TC/Zn(II) onto biochar occurs endothermically in the concentration range studied.[46]

Finally, the magnitudes of the mean adsorption energy (E) derived from the D–R isotherm model were lower than 8 kJ mol^{-1} in both adsorption systems, suggesting that hydrogen bonding, hydrophobic effect, electrostatic attractions and interaction between adsorbate and biochar probably play a significant role during the adsorption process.

3.5 Adsorption thermodynamics

The adsorption nature of single-component and co-adsorption systems was demonstrated by evaluating the changes in Gibbs free energy ($\Delta G°$), enthalpy ($\Delta H°$), and entropy ($\Delta S°$). Table S5† shows the calculated values of the three parameters.

The negative $\Delta G°$ values for both adsorption systems indicated that the adsorption of TC/Zn(II) was thermodynamically spontaneous and favorable. More negative $\Delta G°$ values implied more reliable adsorption driving force at a higher temperature.[47] Moreover, the computations at -20 to 0 kJ mol^{-1} confirmed the physical nature of the adsorption following the D–R isotherm analysis.[48]

The obtained positive $\Delta H°$ values revealed the endothermic nature of TC/Zn(II) adsorption, and high temperature favored the adsorption process. Furthermore, the $\Delta H°$ values were much more than 40 kJ mol^{-1}, which indicated that the chemisorption was dominant in the adsorption process. Finally, the positive $\Delta H°$ values revealed the affinity between the TC/Zn(II) and biochar with an increased degree of freedom as well as increased randomness at adsorbate–solution interface during the adsorption process.[49]

3.6 Mechanism of adsorption

Adsorption kinetics is usually controlled simultaneously by film diffusion and intra-particle diffusion. The single-component
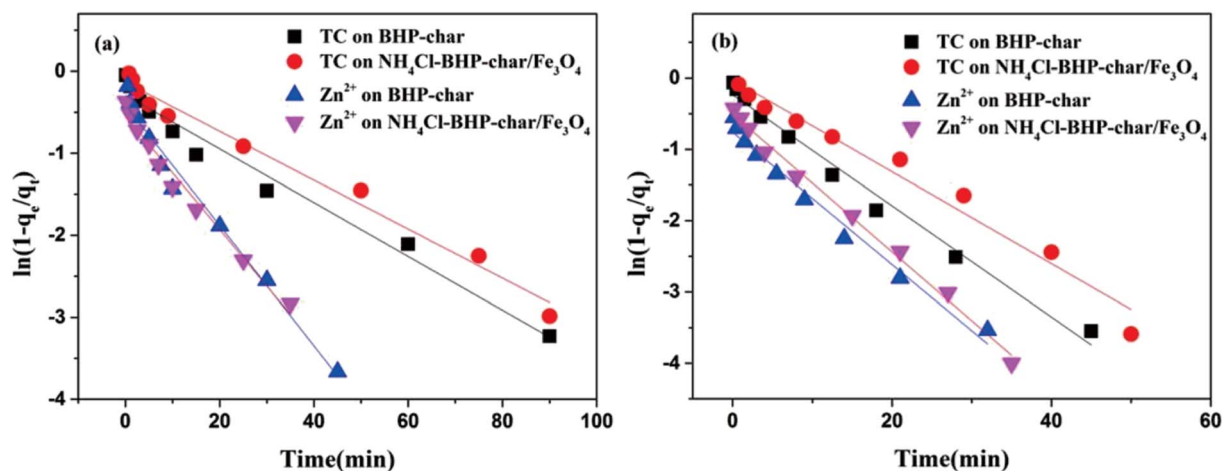

Fig. 4 Film diffusion kinetic plot ((a) single-component adsorption system and (b) co-adsorption system).
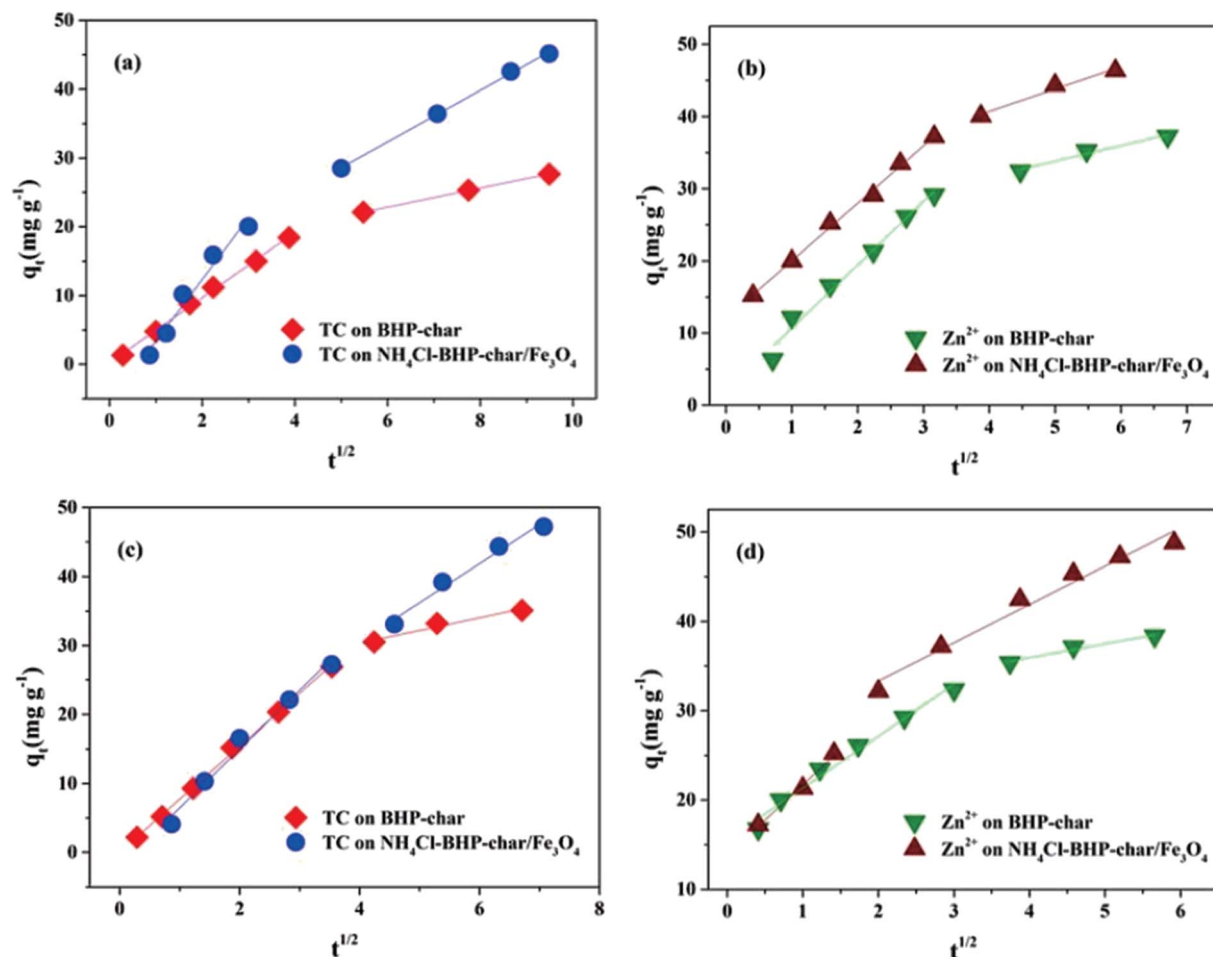
Fig. 5 Intra-particle diffusion kinetic plot ((a and b) single-component adsorption system, (c and d) co-adsorption system).

and co-adsorption behavior of the TC/Zn(II) system are explored using the above two diffusion models to determine the type of rate-controlling step. Fig. 4 and 5 show the plots obtained for film diffusion and intra-particle diffusion models, and Tables S6 and S7† show the related parameters.

In the adsorption systems, the adsorption of TC/Zn(II) on BHP-char and NH$_4$Cl-BHP-char/Fe$_3$O$_4$ mainly exhibited two stages (stages I and II), which was related to the changes in mass transfer rates during the adsorption process.

Stage I represents the rapid adsorption (film diffusion), attributed to the diffusion of TC/Zn(II) through the liquid film surrounding the biochar surface. Although the plots present some linearity ($R^2 > 0.96$), the slope did not cross the origin, attesting the involvement of film diffusion in the adsorption-reaction process.

Stage II was more gradual adsorption (intra-particle diffusion), corresponding to the TC/Zn(II) transport within the inner biochar surface. It was attributed to the higher internal diffusion ability at initial adsorbate concentration.[50] However, the plots did not pass through the origin, which meant the presence of the boundary layer. It was proved that the intra-particle diffusion mechanism was not the rate-determining step.[9,18] Hence, both mechanisms were possible.

The infrared spectra of NH$_4$Cl-BHP-char/Fe$_3$O$_4$ were detected before and after the co-adsorption of TC/Zn(II) (see Fig. S4†) to study the adsorption mechanism. For the infrared spectra of NH$_4$Cl-BHP-char/Fe$_3$O$_4$, the characteristic peak of Fe appeared at 668 cm^{-1}, but the other absorption peaks were not distinct, which indicated the less functional groups on the surface of the modified biochar. The infrared spectra of TC/Zn(II) showed that the broad and intense absorption peak around 3460 cm^{-1} was attributed to the –OH stretching vibration. The peak at 1640 cm^{-1} was assigned to stretching vibration of C=O, and that at 620 cm^{-1} assigned to the deformation vibration of C–H bond. After co-adsorption, there were three peaks in NH$_4$Cl-BHP-char/Fe$_3$O$_4$, namely the –OH stretching vibration peak around 3430 cm^{-1}, the C=O stretching vibration peak at 1620 cm^{-1} and the C–H deformation vibration peak at 614 cm^{-1}. The above results showed that TC/Zn(II) was adsorbed in the inner pores of NH$_4$Cl-BHP-char/Fe$_3$O$_4$ in a denser state.

3.7 Cycle regeneration

For magnetic carbon materials, reusability is critically important to reduce costs and improve adsorption.[51] Four cycles of adsorption–desorption experiments were performed to explore
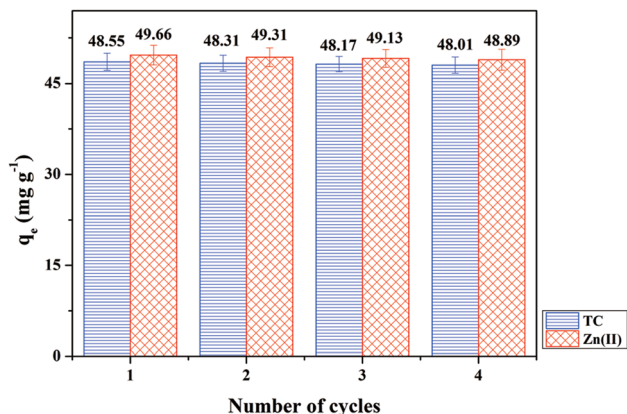
Fig. 6 Reusability of NH$_4$Cl-BHP-char/Fe$_3$O$_4$ for Zn^{2+} and TC removal. Conditions: pH of co-adsorption of TC/Zn(II) was 6.0, initial TC/Zn(II) concentrations 25 mg L^{-1}, adsorbent concentrations 0.5 g L^{-1}, temperature 25 °C, contact time 120 min.

the regeneration of NH$_4$Cl-BHP-char/Fe$_3$O$_4$. Fig. 6 shows that the q_e of NH$_4$Cl-BHP-char/Fe$_3$O$_4$ is essentially unchanged during four adsorption–desorption cycles, indicating NH$_4$Cl-BHP-char/Fe$_3$O$_4$ is efficient, stable, and easy to reuse.

3.8 Cost of adsorbents

The BHP of the cheapest variety cost about CNY 2800 per ton. The modified materials used in the present study were generally available at a relatively cheap rate, CNY 680 per ton for ammonium chloride, and CNY 1600 per ton for magnetite. The finished products cost approximately CNY 3500 per ton for NH$_4$Cl-BHP-char/Fe$_3$O$_4$, including all expenses (transportation, handling, electrical, energy, and drying).

4 Conclusions

This is the first study on the single-component and co-adsorption of TC/Zn(II) (tetracycline and Zn^{2+}) by ammonium chloride-induced magnetic ultra-fine buckwheat peel powder biochar (NH$_4$Cl-BHP-char/Fe$_3$O$_4$). The co-adsorption effect of TC/Zn(II) on NH$_4$Cl-BHP-char/Fe$_3$O$_4$ was better than that of single-component adsorption, and biochar after the adsorption could be separated magnetically. pH 4.0 and 6.5 were optimal for single-component adsorption of TC and Zn(II), respectively, and pH 6.0 was optimal for co-adsorption. In the single-component adsorption system, the rate-limiting step of the adsorption process was the chemisorption.

Compared to the Freundlich isotherm, the Langmuir isotherm could better describe the adsorption behavior, namely monolayer adsorption on a homogenous biochar surface. In the co-adsorption system, physisorption and chemisorption occurred during the adsorption, but the latter occupied a dominant position. The adsorption equilibrium data could be satisfactorily explained by the Freundlich isotherm, indicating that the co-adsorption was multilayer adsorption.

Furthermore, the adsorption rate was jointly controlled by both film diffusion and intra-particle diffusion, and TC and

Zn(II) promoted the adsorption of each other. The thermodynamic parameters of both adsorption systems implied that the adsorption was endothermic and spontaneous under test conditions. Finally, the adsorption–desorption tests showed that NH$_4$Cl-BHP-char/Fe$_3$O$_4$ could be reused at least 4 cycles for removing TC/Zn(II) from the solution.

Conflicts of interest

There are no conflicts to declare.

Acknowledgements

References

1 S. Álvarez-Torrellas, R. S. Ribeiro, H. T. Gomes, G. Ovejero and J. García, *Chem. Eng. J.*, 2016, **296**, 277–288.

2 X. Wang, W. Zhang, Y. Huang and S. Li, *Sci. Total Environ.*, 2004, **325**, 39–50.

3 D. Mackay, D. E. Powell and K. B. Woodburn, *Environ. Sci. Technol.*, 2015, **49**, 11913–11922.

4 D. S. Sholl and R. P. Lively, *Nature*, 2016, **532**, 435–437.

5 A. A. Zamani, R. Shokri, M. R. Yaftian and A. H. Parizanganeh, *Int. J. Environ. Sci. Technol.*, 2013, **10**, 93–102.

6 N. Oyaro, O. Juddy, E. N. M. Murago and E. Gitonga, *J. Food Agric. Environ.*, 2007, **5**, 119–121.

7 Q. Song, Y. Fang, Z. Liu, L. Li, Y. Wang, J. Liang, Y. Huang, J. Lin, L. Hu, J. Zhang and C. Tang, *Chem. Eng. J.*, 2017, **325**, 71–79.

8 E. Tanis, K. Hanna and E. Emmanuel, *Colloids Surf., A*, 2008, **327**, 57–63.

9 S. Álvarez-Torrellas, A. Rodríguez, G. Ovejero and J. García, *Chem. Eng. J.*, 2016, **283**, 936–947.

10 W. H. Tsai, T. C. Huang, H. H. Chen, J. J. Huang, M. H. Hsue, H. Y. Chuang and Y. W. Wu, *J. Chromatogr. A*, 2010, **1217**, 415–418.

11 E. A. Auerbach, E. E. Seyfried and K. D. Mcmahon, *Water Res.*, 2007, **41**, 1143–1151.

12 B. D. Witte, J. Dewulf, K. Demeestere and H. V. Langenhove, *J. Hazard. Mater.*, 2009, **161**, 701–708.

13 H. Chen, B. Gao and H. Li, *J. Hazard. Mater.*, 2015, **282**, 201–207.

14 M. T. Ravanchi, T. Kaghazchi and A. Kargari, *Desalination*, 2009, **235**, 199–244.

15 C. Reyes, J. Fernández, J. Freer, M. A. Mondaca, C. Zaror, S. Malato and H. D. Mansilla, *J. Photochem. Photobiol., B*, 2006, **184**, 141–146.

16 X. H. Wang and A. Y. C. Lin, *Environ. Sci. Technol.*, 2012, **46**, 12417–12426.

17 S. K. R. Yadanaparthi, D. Graybill and R. V. Wandruszka, *J. Hazard. Mater.*, 2009, **171**, 1–15.

18 L. Lonappan, T. Rouissi, S. K. Brar, M. Verma and R. Y. Surampalli, *Bioresour. Technol.*, 2018, **249**, 386–394.

19 S. Li, X. Zhang and Y. Huang, *J. Hazard. Mater.*, 2017, **321**, 711–719.

20 J. L. Martinez, *Science*, 2008, **321**, 365–367.

21 C. Jung, J. Park, K. H. Lim, S. Park, J. Heo, N. Her, J. Oh, S. Yun and Y. Yoon, *J. Hazard. Mater.*, 2013, **263**, 702–710.

22 D. Shan, S. Deng, T. Zhao, B. Wang, Y. Wang, J. Huang, G. Yu, J. Winglee and M. R. Wiesner, *J. Hazard. Mater.*, 2016, **305**, 156–163.

23 M. Kobya, *Bioresour. Technol.*, 2004, **91**, 317–321.

24 T. Li, X. Han, C. Liang, M. J. I. Shohag and X. Yang, *Environ. Technol.*, 2015, **36**, 245–253.

25 R. Wu, J. Qu and Y. Chen, *Water Res.*, 2005, **39**, 630–638.

26 A. Dolatkhah and L. D. Wilson, *ACS Appl. Mater. Interfaces*, 2016, **8**, 5595–5607.

27 O. M. Lemine, I. Ghiloufi, M. Bououdina, L. Khezami, M. O. M'hamed and A. T. Hassan, *J. Alloys Compd.*, 2014, **588**, 592–595.

28 P. Liao, Z. Zhan, J. Dai, X. Wu, W. Zhang, K. Wang and S. Yuan, *Chem. Eng. J.*, 2013, **228**, 496–505.

29 G. Moussavi, A. Alahabadi, K. Yaghmaeian and M. Eskandari, *Chem. Eng. J.*, 2013, **217**, 119–128.

30 T. Ai, X. Jiang, Q. Liu, L. Lv and H. Wu, *Bioresour. Technol.*, 2019, **273**, 8–15.

31 N. Suriyanon, P. Punyapalakul and C. Ngamcharussrivichai, *Chem. Eng. J.*, 2013, **214**, 208–218.

32 H. Zhao, X. Liu, Z. Cao, Y. Zhan, X. Shi, Y. Yang, J. Zhou and J. Xu, *J. Hazard. Mater.*, 2016, **310**, 235–245.

33 J. S. Noh and J. A. Schwarz, *J. Colloid Interface Sci.*, 1989, **130**, 157–164.

34 H. Wu, H. Xie, G. He, Y. Guan and Y. Zhang, *Appl. Clay Sci.*, 2016, **119**, 161–169.

35 A. M. M. Vargas, A. L. Cazetta, M. H. Kunita, T. L. Silva and V. C. Almeida, *Chem. Eng. J.*, 2011, **168**, 722–730.

36 F. Lian, Z. Song, Z. Liu, L. Zhu and B. Xing, *Environ. Pollut.*, 2013, **178**, 264–270.

37 D. Momekova, G. Momekov, J. Ivanova, I. Pantcheva, E. Drakalska, N. Stoyanov, M. Guenova, A. Michova, K. Balashev, S. Arpadjan, M. Mitewa, S. Rangelov and N. Lambov, *J. Drug Delivery Sci. Technol.*, 2013, **23**, 215–223.

38 X. Yu, L. Zhang, M. Liang and W. Sun, *Chem. Eng. J.*, 2015, **279**, 363–371.

39 L. Ji, W. Chen, S. Zheng, Z. Xu and D. Zhu, *Langmuir*, 2009, **25**, 11608–11613.

40 H. Huang, J. Tang, K. Gao, R. He, H. Zhao and D. Werner, *RSC Adv.*, 2017, **7**, 14640–14648.

41 H. Wang, C. Fang, Q. Wang, Y. Chu, Y. Song, Y. Chen and X. Xue, *RSC Adv.*, 2018, **8**, 16260–16268.

42 M. T. Islam, R. Saenz-Arana, C. Hernandez, T. Guinto, M. A. Ahsan, H. Kim, Y. Lin, B. Alvarado-Tenorio and J. C. Noveron, *RSC Adv.*, 2018, **8**, 32545–32557.

43 P. Maneechakr and S. Karnjanakom, *RSC Adv.*, 2019, **9**, 24074–24086.

44 V. Frišták, M. Pipíška, J. Lesný, G. Soja, W. Friesl-Hanl and A. Packová, *Environ. Monit. Assess.*, 2015, **187**, 1–16.

45 A. A. Oladipo, E. O. Ahaka and M. Gazi, *Environ. Sci. Pollut. Res.*, 2019, **26**, 31887–31899.

46 M. Hadi, M. R. Samarghandi and G. McKay, *Chem. Eng. J.*, 2010, **160**, 408–416.

47 W. S. W. Ngah and S. Fatinathan, *J. Environ. Manage.*, 2010, **91**, 958–969.

48 Y. Chao, W. Zhu, X. Wu, F. Hou, S. Xun, P. Wu, H. Ji, H. Xu and H. Li, *Chem. Eng. J.*, 2014, **243**, 60–67.

49 M. J. Ahmed and S. K. Theydan, *Chem. Eng. J.*, 2013, **214**, 310–318.

50 B. Chen, W. Sun, C. Wang and X. Guo, *Chem. Eng. J.*, 2017, **316**, 160–170.

51 Y. Zhou, S. Cao, C. Xi, X. Li, L. Zhang, G. Wang and Z. Chen, *Bioresour. Technol.*, 2019, **292**, 121951.